
Estimation of Near Surface effects

Jan Thorbecke
A.J. Berkhout

3.1 Introduction

The most effective weathered layer correction would be inverse extrapolation through the near surface. Unfortunately this procedure is usually not feasible because the exact model of the weathered layer is not known. The strategy, therefore, is to make reasonable assumptions in such a way that a practical solution converges as close as possible to an acceptable effective solution. We will show that, by making assumptions about the *propagation* behavior of a (synthesized) wave field through the weathered layer, an effective estimation of the influence of the weathered layer on the data can be made. We will use the areal shot record technique to simulate waves (in particular plane waves) which optimally illuminate a selected part of the subsurface. Using this approach and making assumptions about the propagation behavior of these waves through a weathered layer we are able to uncouple the weathered layer effects at the source and receiver side. In this chapter these assumptions are tested and visualized with synthetic examples. Following these assumptions an effective estimation of a weathered layer correction is made for different synthetic models.

3.2 Description of the weathered layer

Because we are aiming at a wave equation based correction of the weathered layer our description of the weathered layer must be in terms of propagation, transmission and reflection operators. According to this choice the description of the weathered layer should be three-fold (see Figure 3.1):

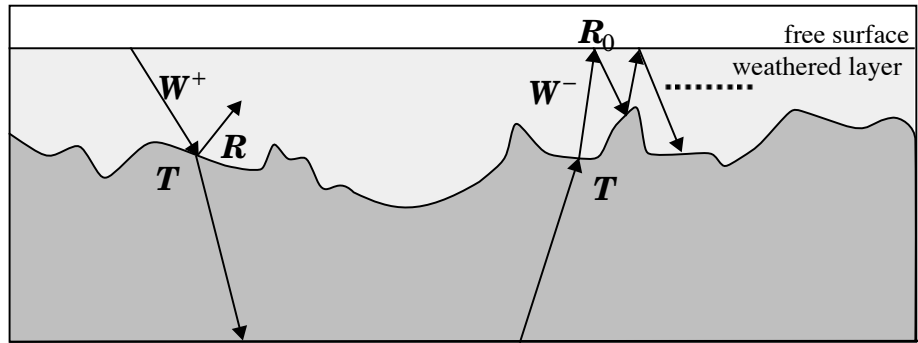


Fig. 3.1 Weathered layer description in terms of propagation, reflection and transmission operators.

- propagation through the weathered layer (\mathbf{W} matrices)
- reflection from and transmission through the weathered layer transition zone (\mathbf{R} and \mathbf{T})
- multiple reflections with the free surface (\mathbf{R}_0 matrix).

From these three effects the *propagation* effects are the main disturbance in the seismic data. In our approach a wave equation based extrapolation operator will be used to estimate and correct this propagation disturbance in the data. The reflection effects, combined with the influence of the free-surface, will be investigated in the near future.

3.3 Weathered layer influence on the Source and Receiver side

A wave emitted by a source at the surface propagates down, gets reflected from deeper interfaces and propagates back to the receiver at the surface. It thus travels at least two times through the weathered layer: the first time when it is emitted by the source and the second time just before it is first recorded at the surface. So the seismic data collects at least two times information of the weathered layer. For example, for *point* sources and *point* receivers a single trace contains information of the weathering around the related source and receiver position.

In Chapter 4 of DELPHI volume 3 we have shown that by using *plane* waves we can, in an intuitive way, estimate the propagation effects of the weathered layer. By using this estimation method an important assumption is made: the main part of the propagation information of the weathered layer can be extracted from the receiver disturbances. This assumption implies that at the source side the weathered layer effects are canceling in the propagation path through the subsurface; the so called ‘healing’ effect on the source side. The first thing we want to do is to clarify and test this assumption. Hence, by using a description in terms of plane waves at the surface it is possible to uncouple the influence of the weathered layer at the source and receiver side.

Assume a plane wave being emitted at the surface. After emission the plane wave travels through the weathered layer further downward. Arriving at a reflector in the *far* field the wave

field has recovered from the disturbed influence of the weathered layer through the long propagation path. After reflection, the reflected wave travels upward. When the reflected wave is near the surface it has to propagate through the weathered layer again before it can be measured by the receivers. In these near surface layers the waves are diffracted (through the relatively fast changing and irregular shape of the weathered layer) and are measured close by: so the receivers measure the *near* field of the weathered layer influence. These important notions, *far* and *near* field, can be explained by using the Rayleigh II integral for a plane surface at $z = z_0$

$$P(\vec{r}_a, \omega) = \frac{1}{2\pi} \iint_S P^+(\vec{r}, \omega) \frac{\partial}{\partial z_0} G(\vec{r}_a, \vec{r}, \omega) dS. \quad (3.1)$$

with

$$\begin{aligned} \vec{r} &= (x, y, z_0) \\ \vec{r}_a &= (x_a, y_a, z_a). \end{aligned} \quad (3.2)$$

The Greens function in the Rayleigh II integral is for a homogeneous isotropic medium, in the space frequency domain, given by

$$G(\vec{r}_a, \vec{r}, \omega) = \frac{e^{-jk|\vec{r}_a - \vec{r}|}}{|\vec{r}_a - \vec{r}|}, \quad (3.3)$$

where $k = \omega/c$ and the distance between the point of measurement and the position to be calculated is

$$\Delta r = |\vec{r}_a - \vec{r}| = \sqrt{((x_a - x)^2 + (y_a - y)^2 + (z_a - z_0)^2)}. \quad (3.4)$$

Calculation of the derivative of the Green's function leads to

$$\frac{\partial}{\partial z_0} G(\vec{r}_a, \vec{r}, \omega) = \frac{\Delta z}{\Delta r} \frac{(jk\Delta r + 1)}{\Delta r} G(\vec{r}_a, \vec{r}, \omega), \quad (3.5)$$

with $\Delta z = z_a - z_0$. Substituting equation (3.5) into equation (3.1) leads to an expression which can be subdivided into two parts:

$$P(\vec{r}_a, \omega) = P^n(\vec{r}_a, \omega) + P^f(\vec{r}_a, \omega). \quad (3.6)$$

The first term in equation (3.6) represents the near field and the second term represents the far field. The near and far wave field are given by the following two expressions

$$P^n(\vec{r}_a, \omega) = \frac{1}{2\pi} \iint_S \frac{\Delta z}{\Delta r} P^+(\vec{r}, \omega) \frac{G(\vec{r}_a, \vec{r}, \omega)}{\Delta r} dS, \quad (3.7a)$$

$$P^f(\vec{r}_a, \omega) = \frac{1}{2\pi} \iint_S \frac{\Delta z}{\Delta r} jkP^+(\vec{r}, \omega) G(\vec{r}_a, \vec{r}, \omega) dS. \quad (3.7b)$$

The near field term will have a small influence in the total field at position \vec{r}_a if Δr has a large value. We want to make the assumption that a plane wave, which has traveled through a complicated weathered layer, can be considered again as a plane wave in the far field. We will test this assumption with some propagation experiments through different weathered layer models.

By considering the propagation effects in the wavenumber-frequency domain we can, in another way, make clear that a disturbed plane wave can be considered again as a plane wave in the far field. We know that a discrete plane wave is in the wavenumber-frequency domain represented by a Dirac comb along the wavenumber axis. We also know that propagation is identical with low-pass filtering in the wavenumber domain (see for example Berkhout, 1987). So the disturbed plane wave in the far field is a low-pass filtered (=propagated) version of the plane wave in the near field. The low-pass filtering has removed all the high angle energy and the propagated part can be considered again as a plane wave.

A set of synthetic experiments is carried out to see the influence of the weathered layer in the far field. The synthetic model consists of two acoustic layers. The contrast between the top layer and the layer below is the same for all experiments. The transition zone between the two layers is modeled with a linear gradient of 10 (m/s)/m. The standard setup for these far field experiments is shown in Figure 3.2 together with the results of a reference model, where the weathered layer transition zone is horizontal. The wavelet we used has a maximum frequency of 30 Hz, so the minimum wavelength in the weathered layer is 30 meters and the minimum wavelength in the lower layer is 80 meters.

The transition zone between the weathered layer and the layer below is for the far field experiments sinusoidally shaped. In Figure 3.3 the results are shown for 6 different transition zones. The wavelength of the sinusoidally shaped interface is changed for the different transition zones. The number above the model indicates the wavelength (in meter) of the transition zone, the ‘amplitude’ of the sinus is for all transition zones 50 meter. In the display the distance between two receivers is 8 meters (modeling and calculations are done with 2 meters distance)

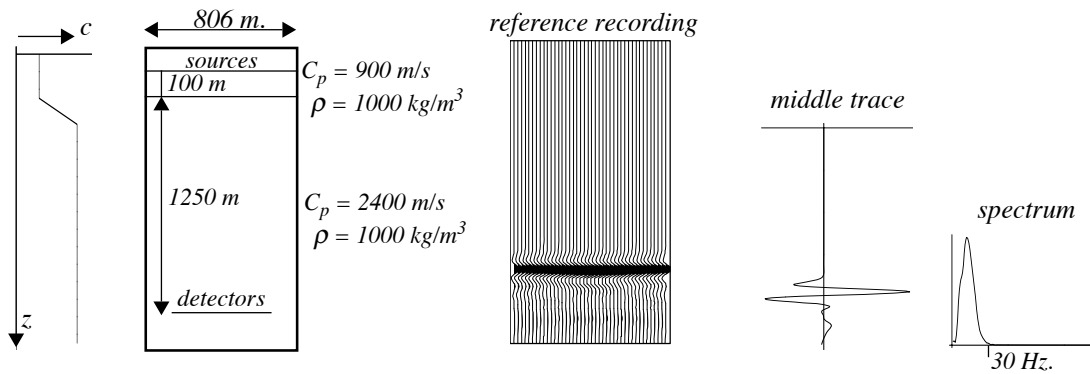


Fig. 3.2 Basic model and reference measurement for testing the far field assumption.

and the time sampling of the recording is 4 ms. The plane wave at the surface is constructed with 400 monopole pressure sources. To decide if the assumption about the healing effect on the source side is acceptable for these synthetic models we have to look at the recorded wave fields shown in Figure 3.3. The recorded wave field, 1350 meters below the sources and 1250 meters below the baseline of the transition zone, shows with respect to travel time for almost all transition zones a plane wave with sometimes a ringing effect in the wavelet. For the transition zones with a rapid horizontal change (small wavelength of the sinusoidally shaped transition zone) we see that the plane wave assumption in the far field is valid. For the slowly varying transition zones (large wavelength of the transition zone) an influence of the model can still be observed in the received far field. So slow lateral variations in the top layers of the earth travel to the far field; fast lateral variations are ‘healed’ in the propagation to the far field. In our

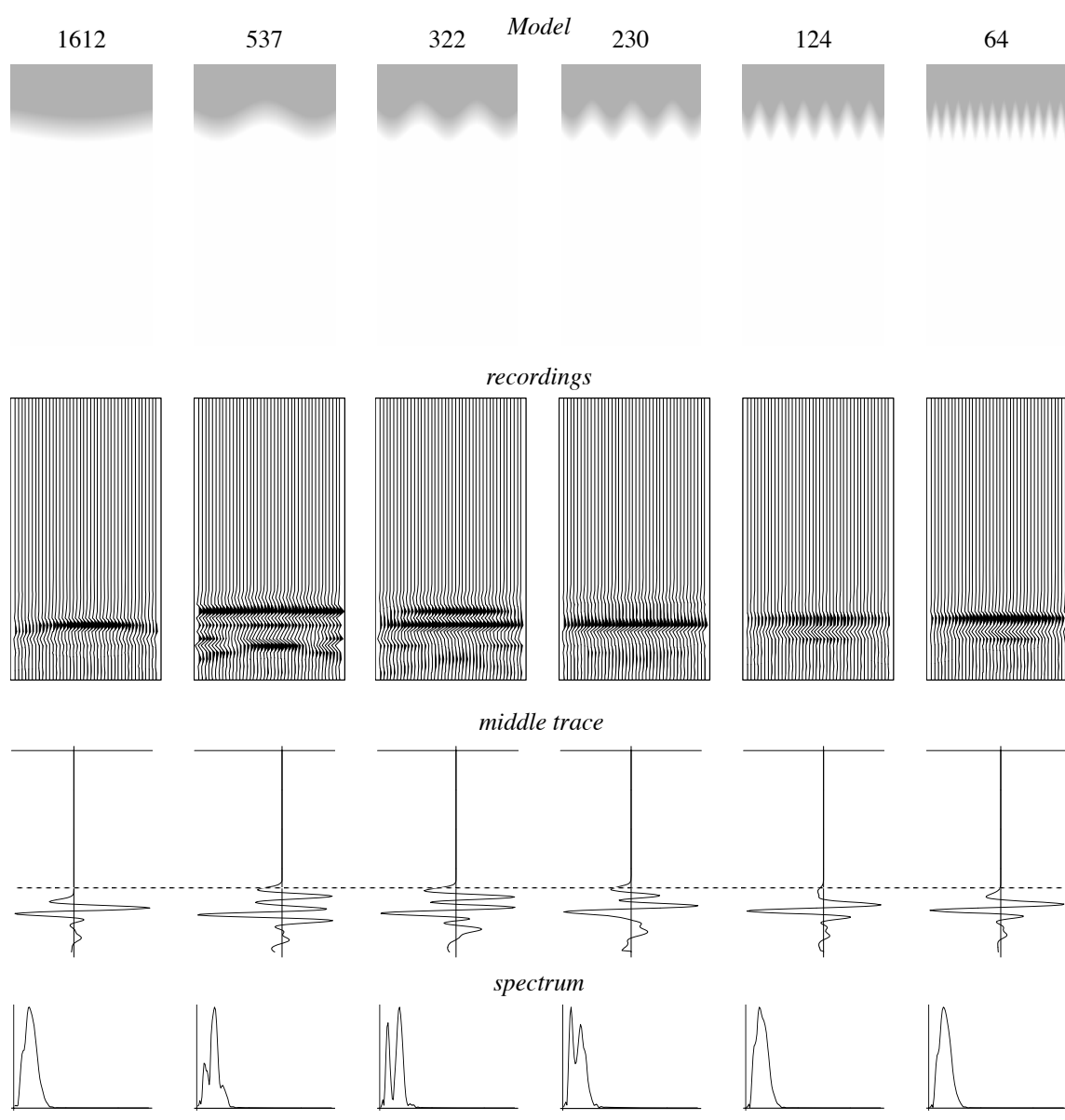


Fig. 3.3 Far field measurements for different weathered layer models (variable spatial periodicity).

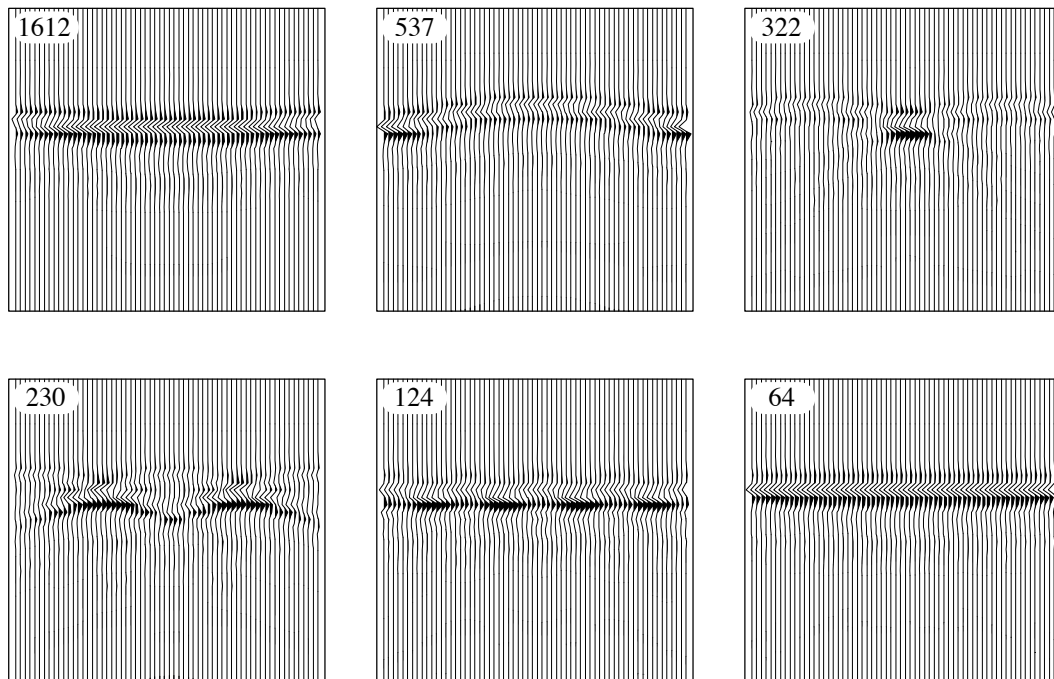


Fig. 3.4 Near field measurements for different weathered layer models (variable spatial periodicity).

approach the change of the plane wave front due to slow lateral variations in the near surface should be included in the macro velocity model. The time function of the middle trace shows that a rapid change in the horizontal direction does not significantly effect the amplitude of the wavelet in the far field (compare with the reference trace in Figure 3.2). It does not effect the wavelet *shape*.

From the examples shown above it is concluded that in the far field most of the near field energy from the weathered layer disturbances cannot be measured anymore. This observation can be used the other way round; in the near field the diffraction information of the weathered layer is still present. We have already mentioned that the receivers at the surface measure the wave field in the near field of the weathered layer diffractions. Thus the near field information of the weathered layer at the detectors will be recorded indeed. Hence, by looking at the influence of the weathered layer on the receiver side we should extract weathered layer information from the data

To see how much information of the weathered layer is in a near field measurement another experiment is carried out. For this experiment receivers are placed at the surface and the plane wave is placed 350 meters below the receivers. The weathered layer models we use are the same as the models for the far field experiments. We have used the same distribution of receivers. The recordings are displayed on a larger scale than the far field experiments in Figure 3.3. In Figure 3.4 the measured wave fields of these experiments are shown. The near field propagation effects of the weathered layer are clearly visible. Comparing these near field measurements with the

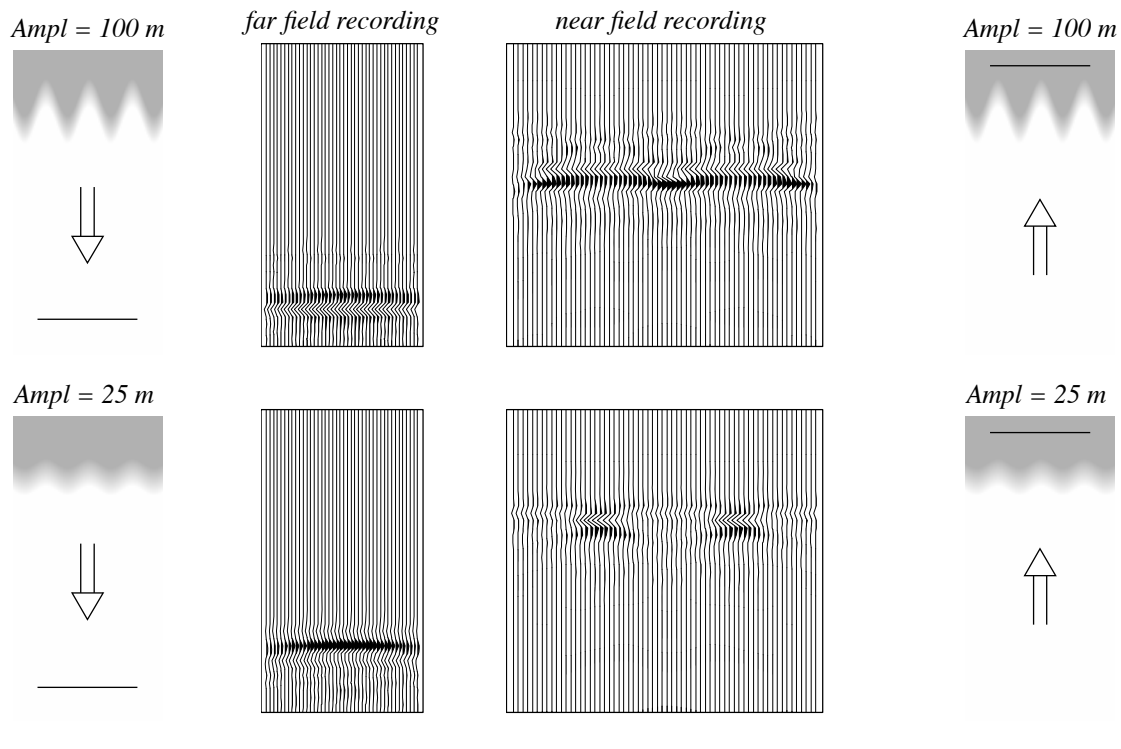


Fig. 3.5 Propagation effects on the source and receiver side for two different amplitudes (irregularities) of the sinusoidal shaped transition zone.

far field experiments we can see that the near field contains much more information about the weathered layer than the far field does. It also shows that a simple static time shift can possibly correct for the diffraction and focussing effects.

Finally some experiments are carried out in which the ‘amplitude’ of the sinusoidally shaped transition zone is changed. The wavelength of the sinusoidal shaped transition zone is chosen at 230 meters and the two ‘amplitudes’ under consideration are 25 and 100 meters. The results of these two experiments are shown in Figure 3.5. It is observed that if the weathered layer transition zone is very irregular (high amplitude) the influence in the near field recordings is significantly stronger than the influence in the far field recording. This observation is in agreement with the previous observation; the near field contains most of the weathered layer information and the weathered layer information in the far field has been dispersed.

The experiments of the far and near field of the weathered layer are used to design a strategy. This strategy is explained, tested and used for a *first* estimation of the weathered layer disturbance.

3.4 Strategy for the estimation of an effective Near Surface model

The upgoing (plane) wave field which arrives at the weathered layer contains all the structural information of the subsurface where it has travelled through. The weathered layer diffractions originating from below the source position at the surface, have been largely ‘healed’ in the long propagation path. When the wave field is recorded *all* the information of the subsurface is distorted in a consistent way due to the irregular weathered layer. In equation (3.8) the upgoing areal wave field just below the weathered layer is written as $\vec{P}^-(z_1)$ and all the propagation effects of the weathered layer are given by $\mathbf{W}^-(z_0, z_1)$,

$$\vec{P}^-(z_0) = \mathbf{W}^-(z_0, z_1)\vec{P}^-(z_1). \quad (3.8)$$

If we use a synthesized plane wave at the surface and assume a very simple subsurface with only one deep reflector (and at the surface a weathered layer), then the upgoing wave field just below the weathered layer is a plane wave. When the plane wave travels upward through the weathered layer it gets diffracted and distorted. By extrapolating the recorded wave field to a datum below the weathered layer we should have a plane wave again if we have used the correct weathered layer model (see also the macro model estimation technique in Chapter 10).

This idea is used and modified to make a first estimate of the weathered layer disturbance. If we have used a correct inverse extrapolation velocity, and the receiver sampling is small enough to record the relevant near field information, then we can for several depth steps calculate the inverse extrapolated wave field. Preferably the inverse extrapolation operator should be accurate for the evanescent wave field as well to restore the evanescent waves to their exact positions in the imaging plane. If we don’t include the evanescent waves the original near field is not reproduced and the image is actually an equivalent field which radiates a far field which is identical to that of the original secondary sources (see Williams, Maynard and Skudrzyk, 1980). Inverse extrapolation, with the well known complex conjugate propagation operator (G^*), has a limited resolution; there can be no spatial variation faster than the minimum wavelength (λ_{min}) and for $\Delta z > \lambda_{min}$ the decay of the evanescent field is so rapid that essentially all of the information for $k_x > k$ is lost. The numerical implementation of a broad band inverse extrapolation operator, which also includes the evanescent waves, will be investigated in the near future. In the remainder of this chapter synthetic experiments are described to test some of the basic ideas in the suggested procedure.

The near and far field experiments shown in the previous section can be combined into one experiment in which both effects are present. For this experiment the same type of weathered layer is used, but now with a strong reflector at 1350 meters below the sources and with the receivers placed at the same positions as the sources. We did this experiment with only one weathered layer model in which the wavelength of sinusoidal shaped transition zone is 230 meters and the amplitude 50 meters. With this experiment we will show that by using the near field information, which originates from the diffractions at the receiver side, we can estimate a first weathered layer model. In Figure 3.6 the snapshots for this experiment are shown. In these

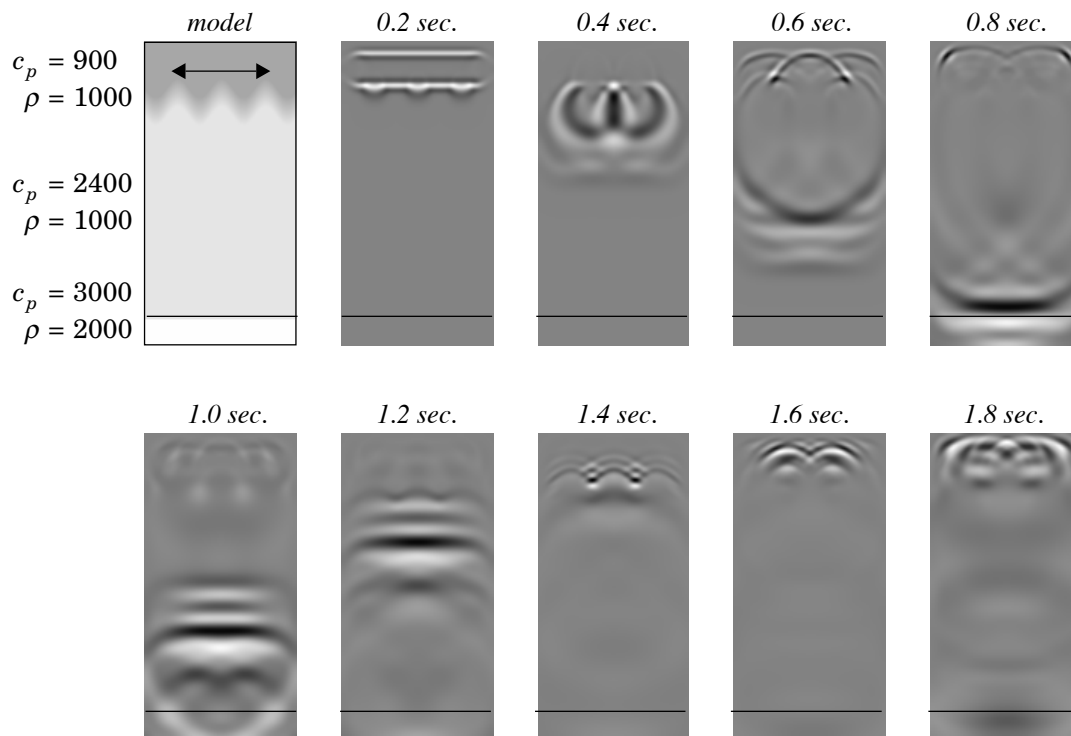


Fig. 3.6 Reflection experiment, including a weathered layer.

snapshots the ‘healing effect’ of the down going wave field is clearly observed. After reflection by the deep reflector the plane wave travels upward and gets distorted by the weathered layer. The large velocity contrast between the weathered layer and the layer below amplifies the weathered layer disturbance even more. In the snapshot at 1.4 seconds a focussing effect is observed in the anticlines of the sinusoidal shaped transition zone. In the snapshot at 1.6 seconds we see that this focussing effect determines the whole picture.

The double arrow shown in the model of Figure 3.6 gives the total length of the receiver spread. The recorded wave field, and a muted version, is shown in Figure 3.7a. In the measurement, shown on the left, three events are observed; the direct wave, the reflections from the weathered layer transition zone and the reflections from the deep reflector (the “target”). In the muted version, the right picture in Figure 3.7a, we have excluded the reflection information of the weathered layer and the direct wave. The remaining reflection data, the right hand-side of Figure 3.7a, shows the deep reflection distorted by the weathered layer. With this remaining data we try to estimate an effective weathered layer model by extrapolating this data, for different extrapolation steps, through a homogeneous medium. For this homogeneous medium we have used the velocity of the weathered layer. If we don’t have a good indication of the velocity in the weathered layer we have to repeat the procedure for different extrapolation velocity values.

To make an estimate of the weathered layer influence, the data is extrapolated for different extrapolation steps. When the diffractions of the weathered layer are in focus a correlation with

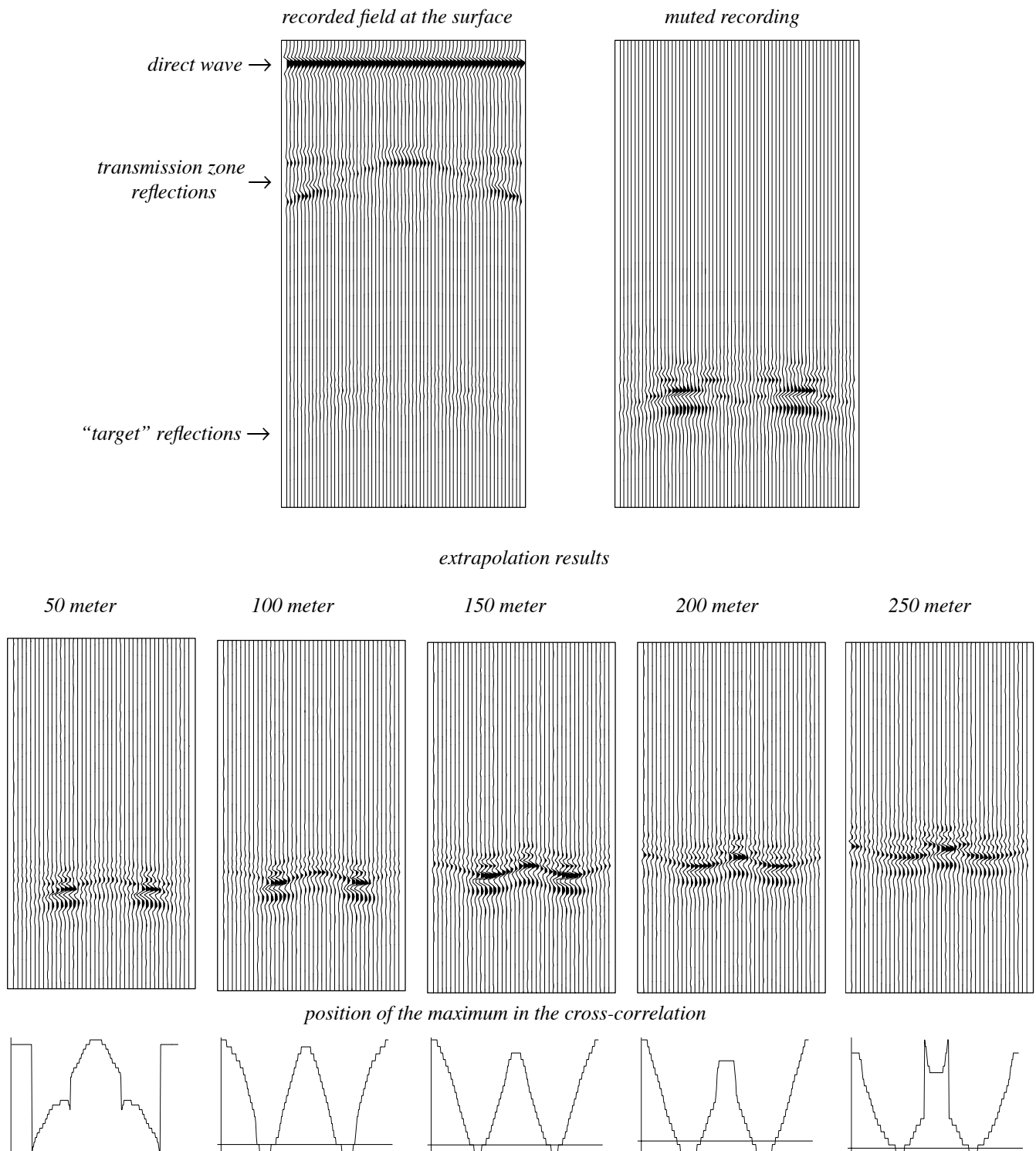


Fig. 3.7 Top: Recorded wave field (left) and a muted version with only the deep reflection data (right).
Bottom: Extrapolated wave field and maximum cross-correlation time lags for different extrapolation steps.

respect to the central trace is carried out (this procedure is equivalent to a cross correlation with a plane wave). From this cross correlation the time lags for the highest amplitudes per trace are picked. These maxima give an indication of the weathered layer model in terms of effective time delays on a extrapolated plane wave. This procedure is shown schematically in Figure 3.8.

The extrapolated results, for five different extrapolation steps, and the maximum time lags of the cross-correlation are shown in Figure 3.7. The diffractions in the records are in focus at an extrapolation step of 100 and 150 meter. The basis of the transition zone lies 100 meter below the receivers, but the transition zone has a linear gradient of 150 meter, which explains the small differences between the different extrapolation steps around 100 meter. From these results we observe that the estimation technique gives a good impression of the propagation behavior of the weathered layer disturbance. The position of the maximum in the cross-correlation gives a first indication of the shape of the weathered layer.

This same experiment is repeated with a dipping reflector at “target” depth. The subsurface model we used is larger than the previous model, to avoid unwanted boundaries effects. In order to be able to compare the results with the previous experiment a selected part of the ‘dipping reflector’ experiment is given. The results of this experiment are shown in Figure 3.9. We observe that the structural information of the subsurface is estimated together with the weathered layer disturbance. In the future we will investigate how we can discriminate between structural information of the subsurface and weathered layer disturbance. We also observe that focussing is still a good criterion for the estimation of propagation effects of the weathered layer.

We have also carried out an experiment in which we have used only one single shot record. The results of this experiment are shown in Figure 3.10. The weathered layer interface is the same as in the previous two models. The deep flat reflector is 1350 below the source position. The model is extended in the x-direction to see more clearly the effect of the curvature of the wave front. The extrapolated recordings for different depth steps show the same behavior for increas-

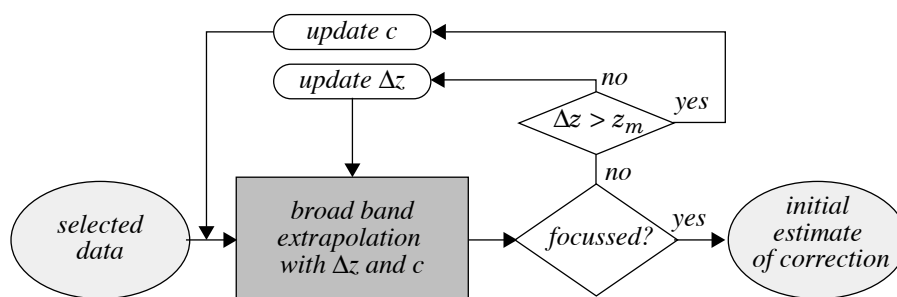


Fig. 3.8 Strategy for the estimation of an effective weathered layer correction.

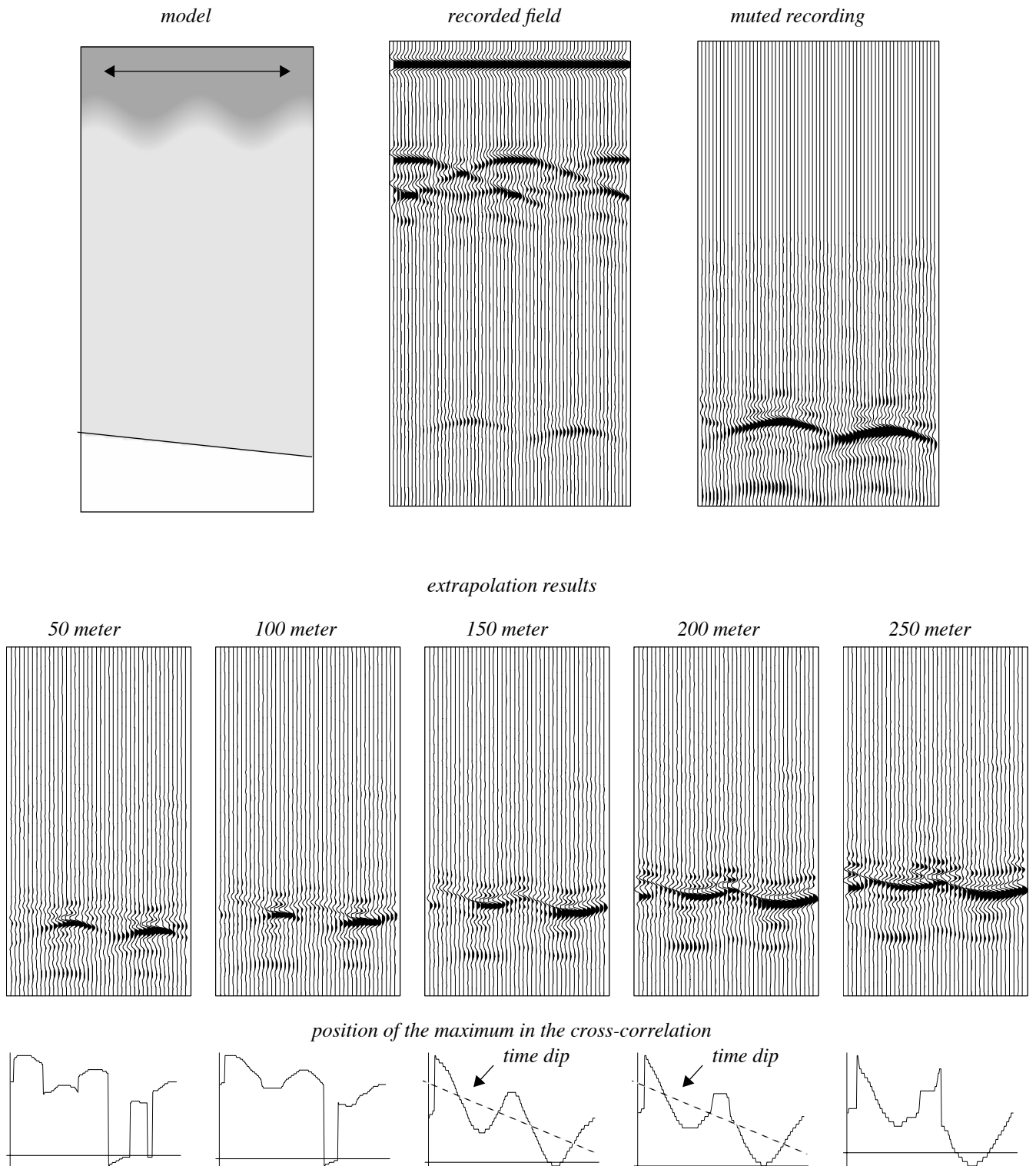


Fig. 3.9 Extrapolated wave field and maximum cross-correlation time lags for different extrapolation steps for a model with a dipping reflector at target depth.

ing depth steps, see Figure 3.11. At a certain depth step the wave field is focussed and a first impression of the weathered layer disturbance can be made. It is observed that the spherical shape of the wave front is estimated together with the weathered layer disturbance. The influence of the distortion of the weathered layer on the source side is different for the plane wave and single shot experiment. This difference is observed in the arrival times of the focussed results. For a plane wave the source side disturbance is a propagation delay originating from a mean position of the weathered layer interface. For a single shot the propagation delay is originating from a local part of the weathered layer interface.

A last test is carried out to see the influence of receiver arrays on the inverse extrapolated results. The same data as shown in Figure 3.10 is used. Every 8 records are added together to produce one single trace (to simulate receiver arrays). With this reduced data set the same procedure is repeated again. The results are shown in Figure 3.12. We observe that the focussing effect is not dramatically effected for an array length of 16 m; the inverse extrapolation result is still acceptable.

The examples discussed above are still acoustic examples. However weathered layer influences are always elastic. We can use the proposed estimation technique also in elastic media if we decompose the elastic data into P- and S-wave potentials. After the decomposition we can use the same acoustic technique on the P and S wave panels. How this decomposition process can be combined with the synthesise procedure is explained in Chapter 9.

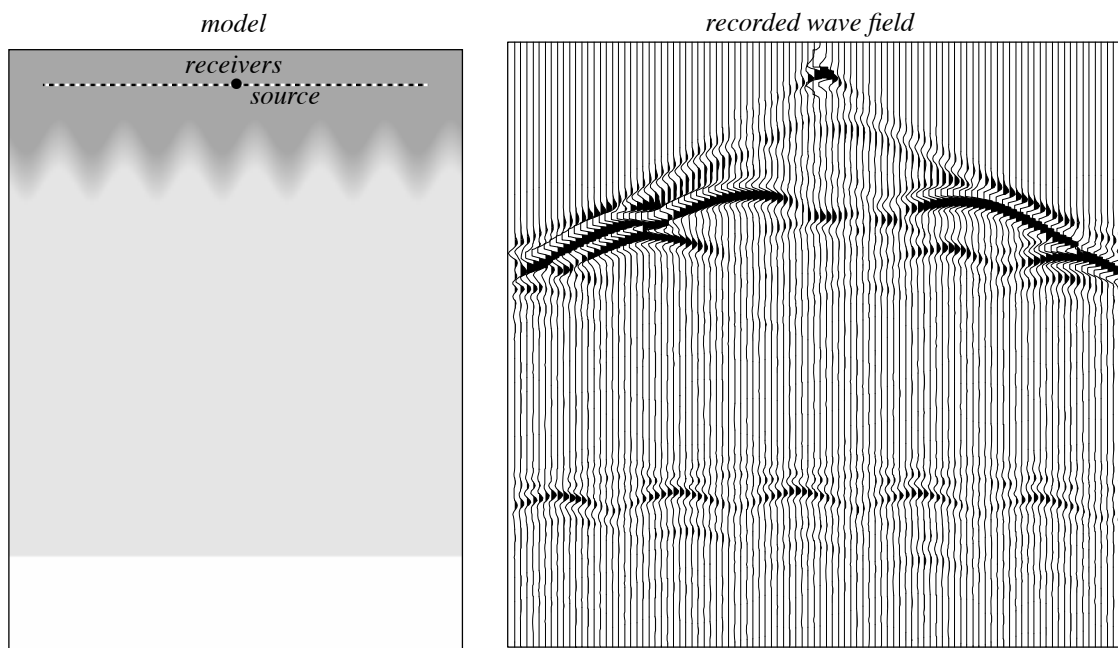


Fig. 3.10 Single shot record experiment; model (right) and surface recording (left).

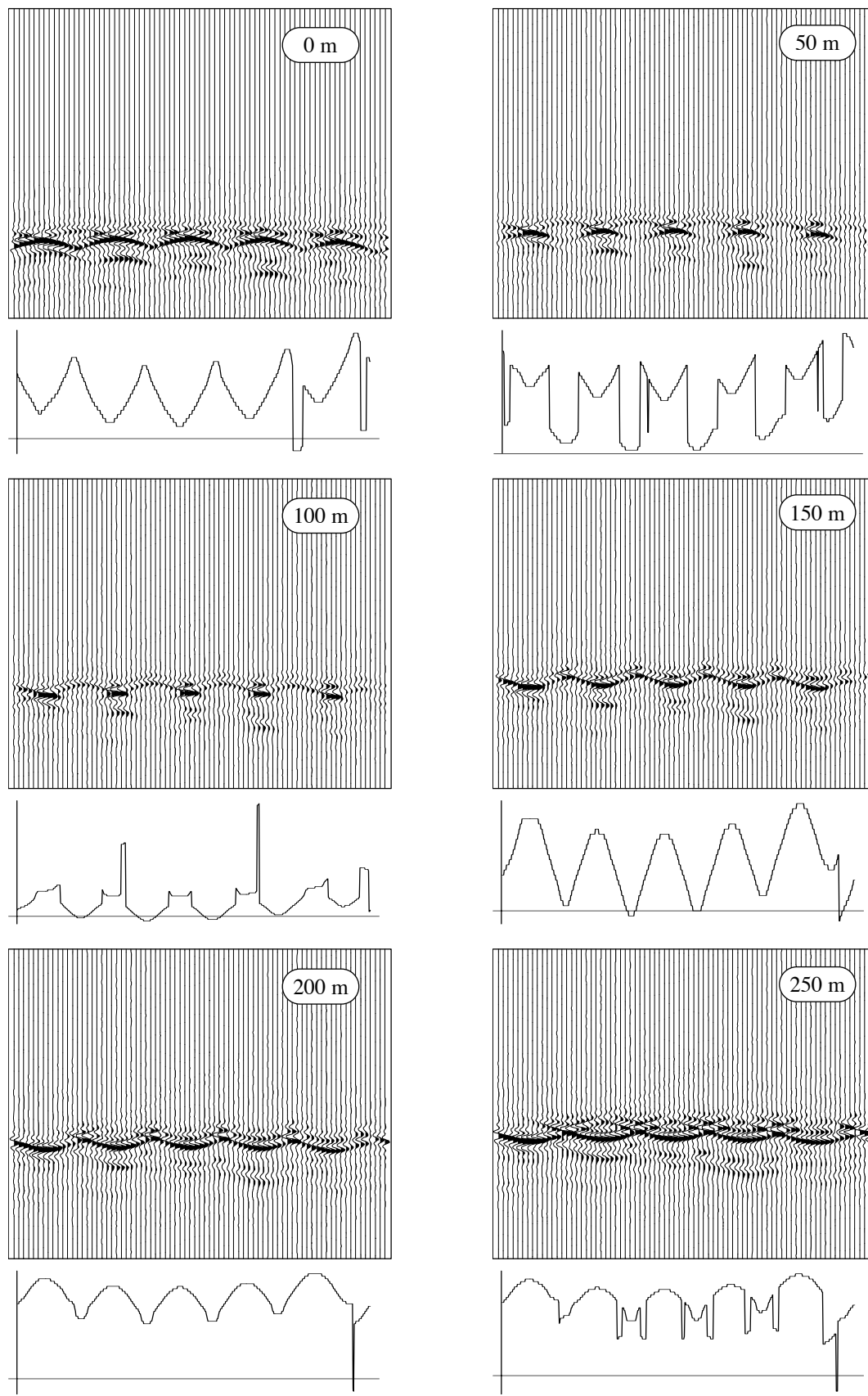


Fig. 3.11 Extrapolation results for single shot experiment.

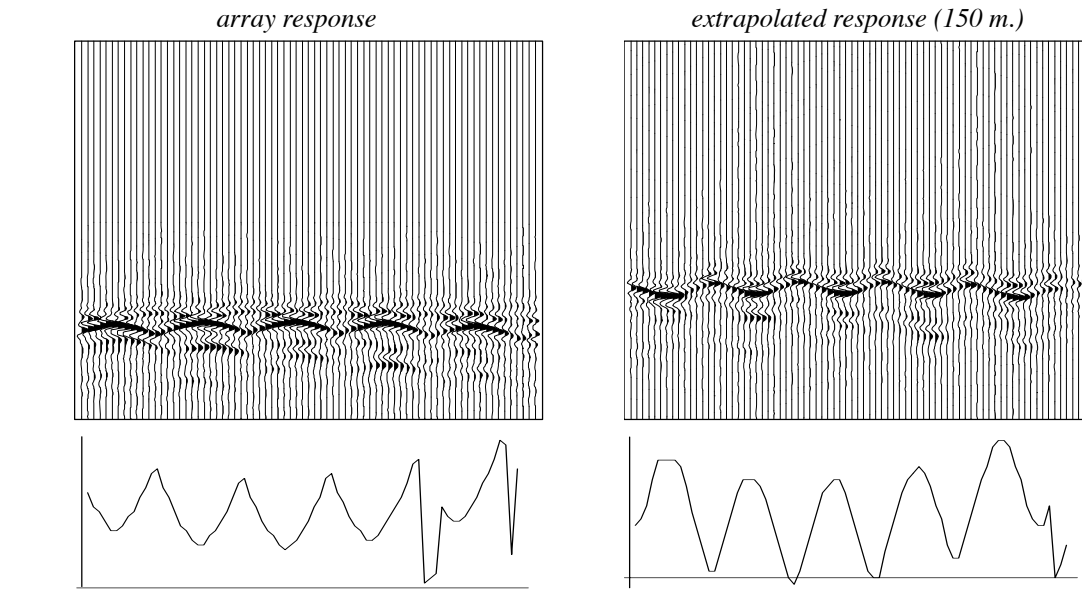


Fig. 3.12 Extrapolation of the single shot data with receiver arrays.

3.5 Conclusions and Future plans

By making reasonable assumptions about the propagation behavior of a (plane) wave through a weathered layer it is possible to uncouple the weathered layer effects at the source and receiver side. The weathered layer distortion to the wave front at the source side are disappearing in the far field, but the near field effects of the weathered layer are measured and can be used in a weathered layer correction technique.

The proposed method uses a downward extrapolation process at the receivers. By focussing the 'mini diffractions' first, we are able to make an initial estimate of the propagation effects in the weathered layer by cross-correlation.

In the future we want use other areal waves types (for example focussing waves) to be able to discriminate more clearly between the structural information of the subsurface and the weathered layer disturbance. We will also concentrate on the development of stable and accurate 'broad band' inverse extrapolation operators to make a better estimation of propagation effects the weathered layer.

Finally, our objective is to integrate the weathered layer problem into a macro model estimation process.

3.6 References

Berkhout, A.J., 1987, *Applied seismic wave theory*, Elsevier Science Publishers, p. 252-255 and p. 279-284

DELPHI, 1990, Progress report Volume I, *From Seismic measurements to rock and pore parameters*, Lab. of Seismics and Acoustics, Delft University of Technology.

DELPHI, 1991, Progress report Volume II, *From Seismic measurements to rock and pore parameters*, Lab. of Seismics and Acoustics, Delft University of Technology.

DELPHI, 1992, Progress report Volume III, *From Seismic measurements to rock and pore parameters*, Lab. of Seismics and Acoustics, Delft University of Technology.

Williams, E.G., Maynard, J.D., and Skudrzyk, E., 1980, *Sound source reconstruction using a microphone array*, JASA, **68**(1), 340-344